

UC Berkeley

UC Berkeley Previously Published Works

Title

Many-to-one function of cat-like mandibles highlights a continuum of sabre-tooth adaptations.

Permalink

<https://escholarship.org/uc/item/1c0176ff>

Journal

Proceedings of the Royal Society B: Biological Sciences, 289(1988)

Authors

Chatar, Narimane

Fischer, Valentin

Tseng, Z

Publication Date

2022-12-14

DOI

10.1098/rspb.2022.1627

Peer reviewed

Research



Cite this article: Chatar N, Fischer V, Tseng ZJ. 2022 Many-to-one function of cat-like mandibles highlights a continuum of sabre-tooth adaptations. *Proc. R. Soc. B* **289**: 20221627.
<https://doi.org/10.1098/rspb.2022.1627>

Received: 18 August 2022

Accepted: 7 November 2022

Subject Category:

Palaeobiology

Subject Areas:

palaeontology, biomechanics, evolution

Keywords:

finite-element analysis, biting simulation, Felidae, Nimravidae, mandible biomechanics, Carnivora

Author for correspondence:

Narimane Chatar

e-mail: narimane.chatar@uliege.be

Electronic supplementary material is available online at <https://doi.org/10.6084/m9.figshare.c.6308901>.

Many-to-one function of cat-like mandibles highlights a continuum of sabre-tooth adaptations

Narimane Chatar¹, Valentin Fischer¹ and Z. Jack Tseng²

¹Evolution and Diversity Dynamics lab, UR Geology, Université de Liège, Building B18, Quartier Agora, Allée du Six Août 14, Liège, 4000, Belgium

²Department of Integrative Biology and Museum of Paleontology, University of California, Berkeley, CA 94720, USA

ID NC, 0000-0003-0449-8574; VF, 0000-0002-8808-6747; ZJT, 0000-0001-5335-4230

Cat-like carnivorans are a textbook example of convergent evolution, with distinct morphological differences between taxa with short or elongated upper canines, the latter often being interpreted as an adaptation to bite at large angles and subdue large prey. This interpretation of the sabre-tooth condition is reinforced by a reduced taxonomic sampling in some studies, often focusing on highly derived taxa or using simplified morphological models. Moreover, most biomechanical analyses focus on biting scenarios at small gapes, ideal for modern carnivora but ill-suited to test for subduction of large prey by sabre-toothed taxa. In this contribution, we present the largest three-dimensional collection-based muscle-induced biting simulations on cat-like carnivorans by running a total of 1074 analyses on 17 different taxa at three different biting angles (30°, 60° and 90°) including both morphologies. While our results show a clear adaptation of extreme sabre-toothed taxa to bite at larger angles in terms of stress distribution, other performance variables display surprising similarities between all forms at the different angles tested, highlighting a continuous rather than bipolar spectrum of hunting methods in cat-like carnivorans and demonstrating a wide functional disparity and nuances of the sabre-tooth condition that cannot simply be characterized by specialized feeding biomechanics.

1. Introduction

A vast series of vertebrate clades have independently evolved sabre-tooth morphologies [1–4]. However, the biomechanical consequences of this trait are poorly known. In cat-like clades (Felidae, Nimravidae and Thylacosmilidae) [5–10], both sabre-toothed and non-sabre-toothed cat-like carnivoran morphotypes are textbook examples of convergent evolution with their own suite of craniomandibular adaptations [3,11–13], the sabre-tooth morphology being often interpreted as an adaptation for subduing large prey [5–10]. However, functional anatomy remains blurry. At first, similar ecomorphologies were suggested for all sabre-tooths clades before some authors highlighted the functional differences between scimitar-toothed and dirk-toothed taxa and, besides, some lineage are extremely convergent with modern ‘conical’ tooth felids (Metailurini and Nimravini) [3,7,11,14,15]. Different hunting behaviours were already proposed for dirk- and scimitar-toothed machairodontines based on FEA simulations [15] but some species considered as ‘mosaic taxa’ (e.g. *Xenosmilus hodsonae* [12]), complexified those models linking form and function. Lautenschlager *et al.* [16] recently highlighted the diversity of mechanical behaviours among sabre-tooth mandibles suggesting that homotherins and metailurins might have use a different bite than smilodontins. Based on a mandibular shape extremely similar to that of extant felines, it was also suggested that primitive machairodontine (*Machairodus aphanistus* and *Promegantereon ogygia*) might also have used a

different bite than more derived sabre-toothed felids [17]. While long-toothed taxa have been widely studied in terms of bending resistance, tooth morphology, gape and post-cranial anatomy [8,10,12,15,16], taxa with shorter canines are often left out of comparative analyses.

The very first study computing finite-element analysis including on cat-like carnivores was published by McHenry *et al.* [18] comparing *Smilodon fatalis* to *Panthera leo* and shown that *Smilodon* head and neck were the most efficient on a restrained prey and concluded that prey had to be brought to the ground before the killing bite. Then, a first attempt of comparing numerous cat-like carnivorous mammals mechanical performances using FEA was made by Piras *et al.* [19] using two-dimensional spline approximation reconstructed from Procrustes coordinates from their geometric morphometric analysis. They found out that sabre-toothed mandibles were more stressed than in modern felines mainly in the ascending ramus [19]. Later, a dirk- and scimitar-toothed cats comparison was published by Figueirido *et al.* [15] comparing *Smilodon fatalis* and a *Homotherium serum* skulls, highlighting high variations between those two machairodontine morphotypes. A comparison between *Smilodon* and *Thylacosmilus* showed that the placental sabre-tooth might not have been the fearsome predator it was thought to be but more of a scavenger [20]. Finally, Lautenschlager *et al.* [16] published a large-scale two-dimensional study comparing all mammalian and non-mammalian sabre-tooths based on two-dimensional outlines using FEA, gape analysis and geometric morphometric. Their results highlighted the high intra and inter clade functional diversity among sabre-tooths predators and are thus an interesting starting point for further analysis [16]. Previous biomechanical simulations on carnivores are often run at gape angle ranging from 25° to 30° a classical angle for modern carnivora [21] that is however ill-suited to test for subduction of large prey by sabre-toothed taxa.

For the first time, we computed three-dimensional biomechanical simulations on a large dataset testing different gape angles including highly derived sabre-tooth taxa (e.g. *Barbourofelis fricki*, *Babrourofelis loveorum*, *Smilodon fatalis*, *Homotherium crenatidens* or *Hoplophoneus primaevus*) but also early machairodontine taxa (e.g. *Paramachaerodus orientalis* and *Machairodus aphanistus*), machairodontines/nimravines taxa which have fairly short upper canines (e.g. *Yoshi minor*) and a wide range of extant felines, in a comparative framework. We also tested different gape angles by performing our analyses at three different gapes: 30°, 60° and 90°.

Here, we thoroughly analyse the biting biomechanics of sabre-toothed and non-sabre-toothed taxa by applying finite-element analyses (FEA) on the largest dataset ever assembled of cat-like placental mandible three-dimensional models, under a variety of gape scenarios. We would have expected taxa with the longest upper canines to be more efficient at larger angles and thus to observe an improvement in the measured performance variables. However, while our results show a clear adaptation of extreme sabre-toothed taxa to bite at larger angles in terms of von Mises stress, other performance variables display surprising similarities between sabre-toothed and non-sabre-toothed forms. The similarities of some performance variables show that the cat-like mandible is an example of ‘many-to-one mapping’ of form–function relationships where forms with obvious morphological disparity produce the same function.

2. Material and methods

(a) Taxonomic sampling

A total of 19 mandibles from 17 different taxa were used to compute the analyses, the complete list of specimens with their metadata is available in table 1.

(b) Preparation of the three-dimensional data

Estimations of the insertion sites of the three main masticatory muscle groups (m. masseter, m. temporalis and m. pterygoideus) requires the cranium and mandible in articulation. However, the cranium of some fossil species may be missing, crushed or incomplete. In these situations where the cranial insertion sites could not be unambiguously placed on the associated skull, we used a cranium belonging to another conspecific or congeneric specimen to get the focal coordinates of muscle origins (see electronic supplementary material, table S1). As routinely employed in FE analyses (e.g. [22–27]), we reconstructed or retrodeformed some models of fossil taxa. To assure transparency, a complete description of the various reconstruction and retro-deformation steps undertaken is available in electronic supplementary material, figures S1–S9. We first computed FEA on two CT-scan based models and then compared our results to those obtained on the same models from which we cleared the internal anatomy to simulate a surface scan-based model. Our results on both type of models were extremely consistent in terms of von Mises stress, mechanical efficiency and adjusted strain energy (see electronic supplementary material, table S2, figures S10–S11) therefore we used only surface scan-based model for the rest of our analysis. This approach is consistent with some recent results showing that surface scans might be a good alternative for CT scans in FEA [28]. The CT-scanned specimens used for the comparison were *Lynx rufus* FAVE09 and *Panthera pardus* AMNH-113745. The CT scan for *Lynx rufus* FAVE09 was obtained from the University at Buffalo Clinical and Translational Science Institute Imaging Center on a GE Discovery 690 PET-CT scanner. The scans of *Panthera pardus* AMNH-113745 and *Smilodon fatalis* AMNH-14349 were initially published in [24] and were scanned in the AMNH Microscopy and Imaging Facility on a General Electric high resolution X-ray micro-CT scanner. For CT scanning parameters see electronic supplementary material, table S3. Image stacks were imported in Avizo lite 2020 (Thermo Fisher Scientific, USA) and region of interest were segmented and exported in STL (STereoLithography) format. Most of the surface scans were obtained with a Creaform HandySCAN 300 laser surface scanner with a resolution varying from 0.2 to 0.5 mm (see electronic supplementary material, table S4). Raw surface scans were then treated using the VX Models software (Creaform, USA) and GeoMagic wrap 2020 (3D Systems, USA) then each part was exported in STL. We measured functional ratios that are commonly considered as sabre-tooth features: coronoid process height and the upper canine length; using the GOM Inspect suite 2018 (Gesellschaft für Optische Messtechnik, Germany, 2018) (see electronic supplementary material, figure S12).

Then, each three-dimensional model was imported in Geomagic Wrap 2020 (3D Systems, USA) and processed. Mandibles were decimated to approximately 150 000 triangles (see electronic supplementary material, table S5) and their XYZ coordinate systems were standardized. Models of the cranium and mandible were articulated at 30°, 60° and 90° of gape angle, providing three biting scenarios for each specimen. On each mandible three muscles groups (*M. temporalis*, *M. masseter* and *M. pterygoideus* groups) were drawn on each side (six muscle attachment regions in total) using GeoMagic (electronic supplementary material, figure S13).

Table 1. Specimens used to compute the FE analyses. Institutional abbreviations: AMNH American museum of Natural History (New York, USA), DNMNH Ditsong National Museum of Natural History (Pretoria, South Africa), PMU Paleontological Museum Uppsala universitet (Uppsala, Sweden), UCMP University of California Museum of Paleontology, FAVE Lab Functional anatomy and vertebrate evolution Lab (Berkeley USA), NHMLA: Natural History Museum of Los Angeles County (Los Angeles, USA), NHMUK: Natural History Museum (London, UK), MNHN Muséum National d'histoire Naturel (Paris, France), NRM Naturhistoriska riksmuseet (Stockholm, Sweden), UF University of Florida (Gainesville, USA). Upper canine ratio = length of the upper canine/cranial length.

subfamily	species	upper canine ratio	cranial length (mm)	specimen no	age	holding institution
Felinae	<i>Caracal caracal</i>	0.12	110.01	A58401	extant	NRM
	<i>Lynx rufus</i>	0.13	81.51	FAVE09	extant	FAVE Lab
	<i>Panthera pardus</i>	0.15	175.25	AMNH-113745	extant	AMNH
	<i>Panthera onca</i>	0.17	217.53	MNHN-ZM-MO-2006-641	extant	MNHN
	<i>Panthera tigris</i>	0.17	315.68	MNHN-ZO-AC-1931-60	extant	MNHN
	<i>Prionailurus rubiginosus</i>	0.12	83.74	MNHN-ZM-MO-2012-54	extant	MNHN
Machairodontinae	<i>Amphimachairodus palanderi</i>	0.26	271.98	PMU-21831	late Miocene	PMU
	<i>Dinofelis barlowi</i>	0.23	257.07	DNMNH-BF-55-23	early Pliocene	DNMNH
	<i>Homotherium crenatidens</i>	0.30	330.36	MNHN-F-PET2000	early Pleistocene	MNHN
	<i>Machairodus aphanistus</i>	0.28	336.27	NHMUK-PV-M37356	late Miocene	NHMUK
	<i>Paramachaerodus orientalis</i>	0.20	174.74	NHMUK-PV-M-8959b	late Miocene	NHMUK
	<i>Smilodon fatalis</i>	0.49	330.72	AMNH-14349	late Pleistocene	AMNH
	<i>Yoshi minor</i>	0.19	149.52	PMU-21766/2	late Miocene	PMU
	Nimravinae	<i>Hoplophonus primaevus</i>	0.34	170.55	LACM-42890	late Eocene
<i>Dinictis felina</i>		0.26	160.70	LACM-162986	late Eocene–mid Oligocene	NHMLA
Barbourofelinae	<i>Barbourofelis fricki</i>	0.74	289.09	UCMP-124942	late Miocene	UCMP
	<i>Barbourofelis loveorum</i>	0.35	258.04	UF-VP-36855	late Miocene	UF

(c) Meshing and FEA protocol

To estimate the forces (Newtons) pulling each muscle insertion, the insertion area (mm^2) was multiplied by 0.3 N mm^{-2} based on the maximum tension produced by mammalian muscle fibres [29]. All biting simulations were unilateral (left and right side were simulated in different scenarios) so to compensate the balancing side muscle forces were multiplied by 0.6 of working side muscles, following [30]. All mandibles were considered isotropic material; a young's modulus of 18 GPa and a Poisson's ratio of 0.3 were defined according to [31–34].

Solid meshes of the mandibles were generated in the Strand7 FE analysis software (Strand7 Pty Ltd, Australia) using four-noded tetrahedral 'brick' elements after an automated mesh 'cleaning' to remove any duplicated nodes. For each specimen, we produced three solid meshes with a coarse-, a medium- and a fine-resolution, respectively, following [25]. Forces were distributed on the muscle insertions in a tangential traction scenario implemented in the Boneload MATLAB routine written by [35] which we slightly modified to adjust the pressure magnitude. The nodal constraint created on the tip of each tooth to simulate each bite scenarios was restrained in the three axes. To avoid free-body movement or over-constraint of the models [36], a nodal

constraint was added on each of the temporomandibular joints (TMJ) preventing any dorsoventral or rostrocaudal movement but still allowing a certain degree of bending of both hemimandibles one towards the other in the mediolateral axis. Then, the linear static solver provided in Strand7 was used to solve the muscle loading model. For model comparison, we extracted different performance variables: the mechanical efficiency, adjusted strain energy and von Mises (VM) stress (see electronic supplementary material for more details about the performance variables and the corrections applied to account for allometric variation in the dataset). Finally, the 'graph' tool in Strand7 was used to measure VM stress values across the mandibles by drawing a line from the middle of the symphyseal region to the base of the coronoid process on both the balancing and working side to obtain values over the whole bone while avoiding areas of unrealistic high stress values near nodal constraints. Then we plotted the rolling mean with a window width of 10 to visualize the evolution of VM stress more smoothly. The elongation of the upper canines and the reduction of the coronoid process are key, convergently evolved sabre-tooth characters [3]. While elongated upper canines is the most striking sabre-tooth trait it implies a reduction of the coronoid process for the animal to open its jaw at a larger angle in

order to clear the elongated upper canines to bite. We looked at the potential correlation between those two typical sabre-tooth features and the VM stress using linear regressions (see electronic supplementary material, for more details).

The three different gape angles, using three different mesh resolutions, as well as on three to four different biting points (depending on the number of teeth) on 19 specimens resulted in a total number of analyses of 1074. All the plots and statistical tests were performed in the R statistical environment version 4.1.0 [37] using different packages [38–46] (see electronic supplementary material for more details).

(d) Phylogenetic signal

To test for the presence of a phylogenetic signal in our results and visualize the distribution of some of the performance variables measured in our analyses, we built a composite phylogeny based on the publications [47–49]. See the electronic supplementary material for additional information on the construction of the tree.

3. Results

(a) Distribution and fluctuation of stress

Our von Mises stress contour plots for a bite simulated on the lower canine (figure 1 for von Mises contour plots of a subset of our dataset and electronic supplementary material, figure S14) show a clear difference between taxa with long and short upper canines. For each angle, regions of high stress are larger (figure 1) and stress is globally higher (electronic supplementary material, figure S14) in taxa with shorter canines within the same clade (see *Machairodus aphanistus* versus *Homotherium serum*; *Dinictis felina* versus *Hoplophoneus primaevus*). At a 30° angle, the lowest stress is observed in *Barbourofelis fricki*—the most derived taxa in terms of sabre-tooth characters [3]—and the highest in the extant *Caracal caracal* (figure 1 and electronic supplementary material, figure S14). Globally, felids display higher stress and larger high-stress areas than nimravids. In taxa with short upper canines, there is a high stress area in the coronoid process of the working side at a 30° angle, this stress being better distributed on the balancing side at 60°. Taxa with long upper canines show a global decrease of the stress at larger angles, yet without important redistribution of stress in other regions of the mandible, except in *Barbourofelis fricki* where the stress is projected more ventrally at larger angles but remains on the working side. While a decrease in global stress is generalized in taxa with the longest upper canines (*Smilodon fatalis*, *Homotherium crenatidens*, *Barbourofelis fricki*, etc.), it peaks at 60° in the others (e.g. *Caracal caracal*, *Panthera tigris*, *Prionailurus rubiginosus*, etc.) and drops drastically at 90°, although those taxa were not mechanically able to open their jaw at such an angle because of the high coronoid process [13]. In that sense, early machairodontines (*Paramachairodus orientalis* and *Machairodus aphanistus*) and taxa considered as ‘cheetah-like’ taxa (*Yoshi minor*) show a different, ‘intermediate’ mandibular mechanical behaviour: stress is redistributed on the balancing side at 60° but remains constant on the working side while decreasing on the balancing one at 90°. We obtained little differences when simulating biting on the lower first molar (electronic supplementary material, figures S15 and S16); the high stress region on the ventral border of the mandible is projected posteriorly on the mandible. In that scenario also, the stress constantly decreases from 30° to 90° in sabre-tooth taxa while showing a peak at 60°

for taxa with shorter upper canines before decreasing at a 90° gape angle. Globally, the stress is higher in smaller taxa and decreases when body size increases within felines (figure 1; electronic supplementary material, figures S17–S18).

The evolution of stress across the mandible is somewhat similar for a canine or a molar bite although sometimes slightly higher in molar bite scenarios (e.g. electronic supplementary material, figures S14A and S15A). Nimravids clearly exhibit lower stress value than felids and felines display higher stress values than machairodontines. The two exceptions in our dataset are *Yoshi minor*, displaying some of the highest stress values recorded (figure 2) and *Paramachairodus orientalis*, which shows stress values comparable to those of *Yoshi minor* but solely on the balancing side, at a 30° (electronic supplementary material, figures S14B and S14B). The highest stress is usually measured at the base of the coronoid process (electronic supplementary material, figures S14 and S15). In some taxa, however (felines, *Yoshi minor* and *Dinictis felina*), stress peaks in the third quarter of the mandible corresponding to a position somewhere below the third lower premolar. While stress is generally extremely low in *Barbourofelis* spp. at a 30° angle it approaches zero at a 90° angle (e.g. minimum measured on the balancing side at 90° for a canine bite 0.18782315). Contrary to what would have been expected the symphysis region does not concentrate lots of stress during the bite; this could be explained by our modelling approach since we did not consider symphyseal material properties, which can have an influence on biomechanical behaviour [50].

(b) Regressions between the stress measured and functional ratio

We test how the von Mises stress correlates with sabre-tooth traits (figure 2; electronic supplementary material, figures S19–S21). There is a negative relation between canine length and the mean von Mises stress measured across the mandible for canine (figure 2) and molar bites (electronic supplementary material, figure S19); unusual taxa such as *Yoshi minor* and *Prionailurus rubiginosus* undeniably lower the adjusted R squared. There is also a discernible positive relation between coronoid height and von Mises stress, even if again *Yoshi minor* reduces the adjusted R squared (electronic supplementary material, figures S20 and S21). From those plots, it is also clear that the mean stress tends to increase at larger angles on the balancing side, while it decreases on the working side suggesting an increasing torsion resulting in a destabilization of the jaw during the bite as previously suggested by Greaves [51]. The Phylogenetic generalized linear models showed that the ML estimate was not significantly different from 0, nor from 1 for all the angle tested, on both the balancing and working side. Overall, there is indeed a correlation between the stress in the mandible and the sabre-tooth trait measured that is not simply due to share ancestry.

(c) Mandible performance

At all the angles measured, both the adjusted strain energy (SE) and mechanical efficiency (ME) are stable in our dataset (electronic supplementary material, figures S22 and S23). At a 30° angle (electronic supplementary material, figures S22A–B and S23A), *Barbourofelis fricki* displays the lowest adjusted strain energy in the dataset (below 0.05) while the highest

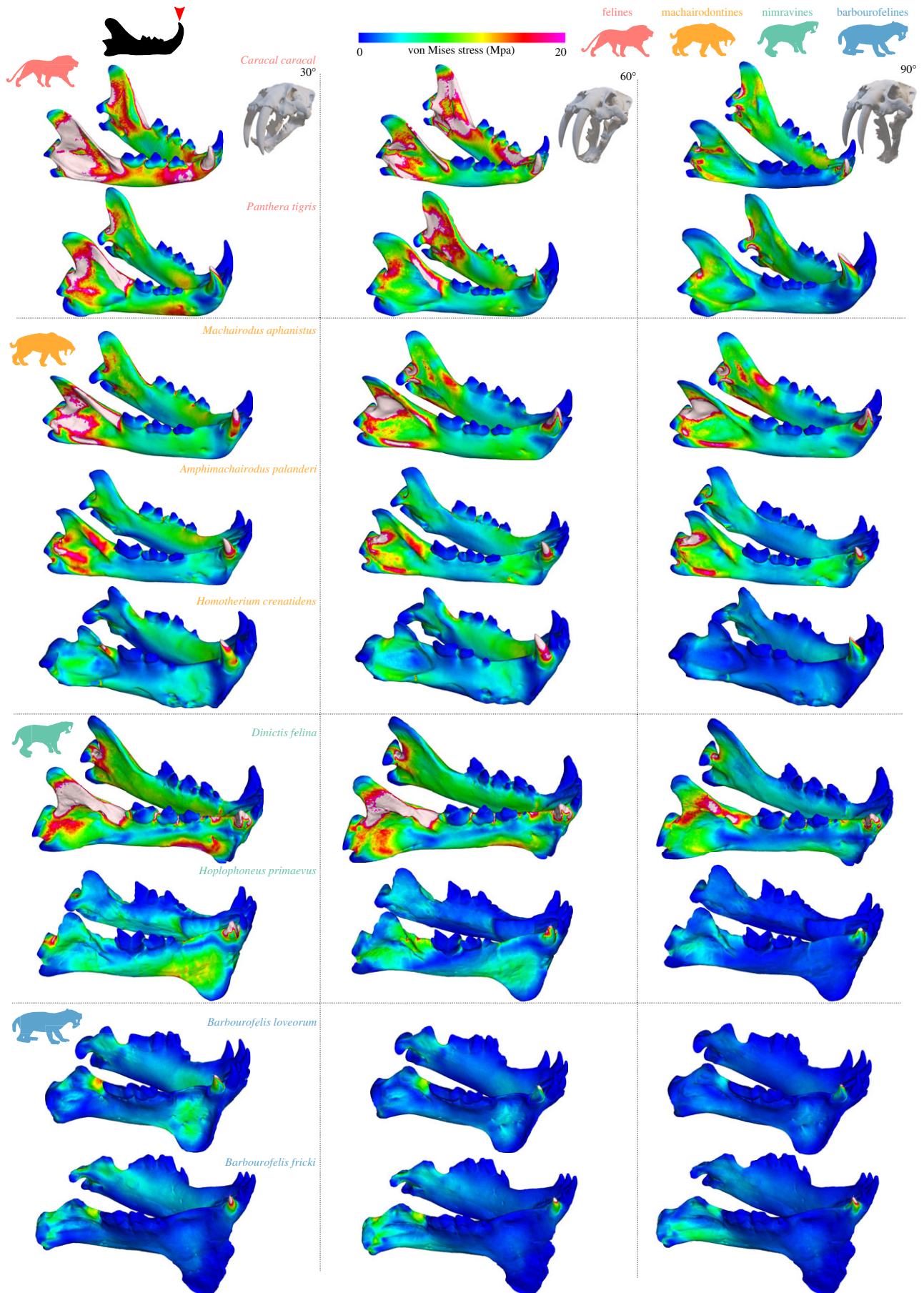


Figure 1. von Mises stress contour plots on nine different taxa at the three different angles for a canine bite. This only show a subset of the complete dataset (17 taxa). (Online version in colour.)

was measured in the machairodontine *Yoshi minor* (from 0.12 to 0.15). Taxa with longer upper canines tend to show lower values of adjusted SE although some extant felines also

occupy the low adjusted SE values on the plots (*Panthera tigris*, *Prionailurus rubiginosus*, *Caracal caracal* and *Lynx rufus*). Mechanical efficiency is relatively stable in our dataset but it

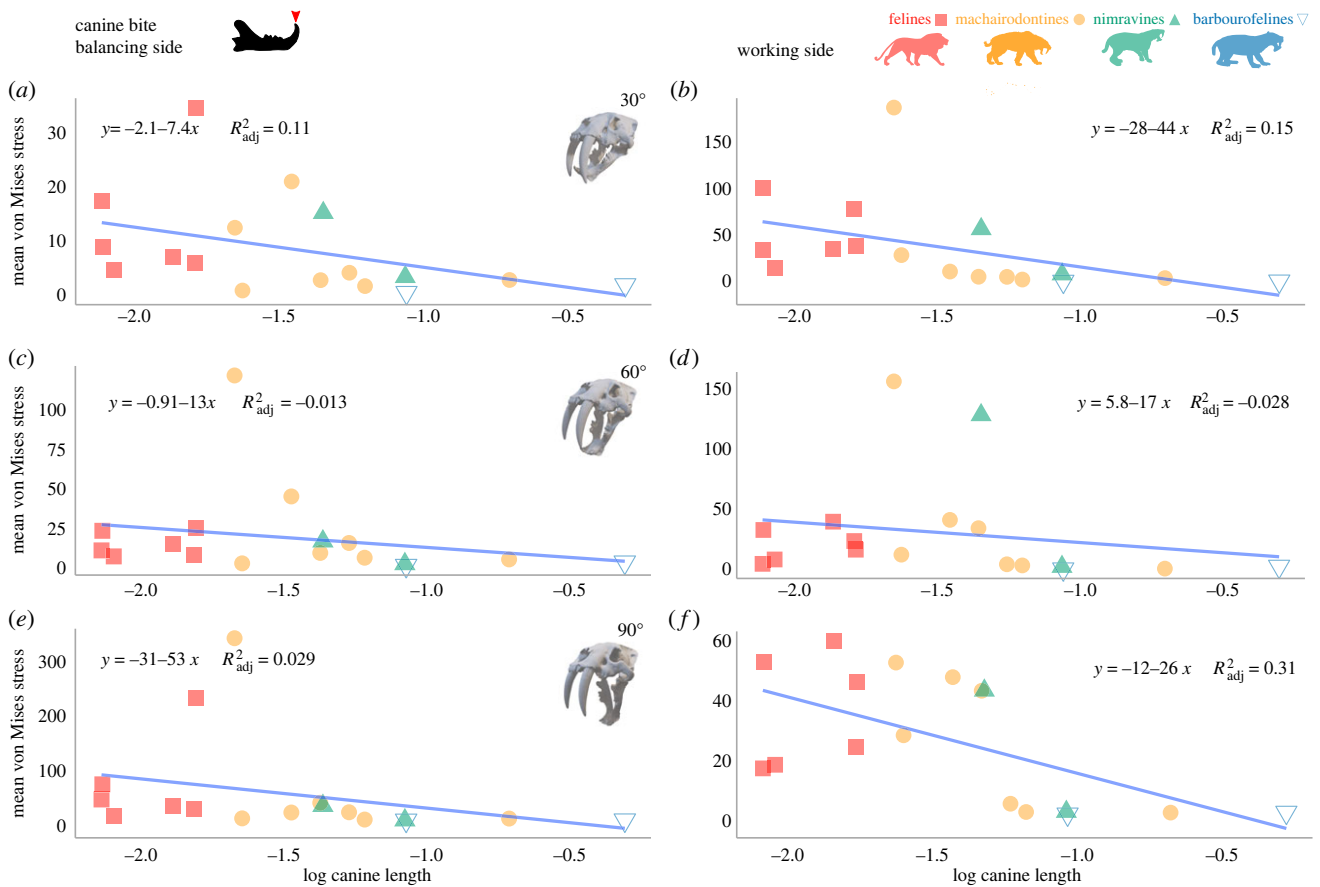


Figure 2. Regressions between the log canine length and the mean von Mises stress measured across the mandible at 30° (a,b), 60° (c,d) and 90° (e,f) for a canine bite in both the balancing (a,c,e) and the working side (b,d, f). (Online version in colour.)

can still be noted that *Smilodon fatalis* explored the widest range of values. At a 60° (electronic supplementary material, figures S22C-D and S23B), the highest and lowest adjusted strain energy are measured in felines, *Panthera pardus* and *Prionailurus rubiginosus*, respectively, while there is no clear tendency for the mechanical efficiency. Finally, at the largest gape angle tested (90°) (electronic supplementary material, figures S22E-F and S23C), the highest adjusted strain energy is measured in *Yoshi minor* and the lowest in the nimravine *Hoplophoneus primaevus*. The nimravine *Dinictis felina* exhibit the highest mechanical efficiency. MANOVA performed on the adjusted strain energy and mechanical efficiency at the three different angles could not recover statistical differences between the families (Felidae and Nimravidae) (p -value at 30° = 0.9718, p -value at 60° = 0.2777, p -value at 90° = 0.0956). Overall, both the adjusted strain energy (electronic supplementary material, figures S24 and S25) and mechanical efficiency (electronic supplementary material, figures S26 and S27) decrease at larger gape angles whether for a canine (figure 3; electronic supplementary material, figures S24 and S26) or a molar bite (electronic supplementary material, figures S25 and S27). Furthermore, performance variables (SE and ME) do not correlate with upper canine length (symbolized by the point size on electronic supplementary material, figures S22 and S23).

The phylogenetic signal for the mechanical efficiency is insignificant for a bite at 30° and 60° but slightly increases at a 90° gape angle. The phylogenetic signal is negligible for the adjusted strain energy at a 30° and 60° bite and remains weak at the 90° bite (Pagel's Lambda and p -values can be seen in table 2).

4. Discussion

Our analyses indicate that the sabre-tooth/non-sabre-tooth dichotomy is actually weak for mandibles which was already suggested in previous biomechanical simulations [15,16]. Indeed, a first study highlighted functional differences between *Homotherium* and *Smilodon* suggesting different hunting behaviour for dirk- and scimitar-toothed cats [15] which is supported by biomechanical analyses on post-cranial bones [52]. An even more recent one dealing with a larger dataset [16] highlighted an even greater functional disparity in the cat-like mandible showing that metailurins had a mechanical behaviour somewhere in between homotherins and pantherins. Globally, species with the longest upper canines are better suited for a bite at larger angles (decreasing von Mises stress values; see figure 1; electronic supplementary material, figures S15–S17) as previously inferred, but more importantly our new data demonstrate there is no clear dichotomy between 'long upper canines' and 'short upper canines' with instead a continuum of biomechanical responses. Part of this continuum of biomechanical responses is driven by varying stress distribution in the working and balancing side in our dataset highlighting the importance of using both hemimandibles for FEA in order to detect such differences in balancing-working side stress response.

(a) Mandibular stress is reduced at higher gape angles

The canine shear bite has been accepted as the typical sabre-tooth killing method in opposition to the feline killing bite [6]. However, biomechanical simulations and morphological

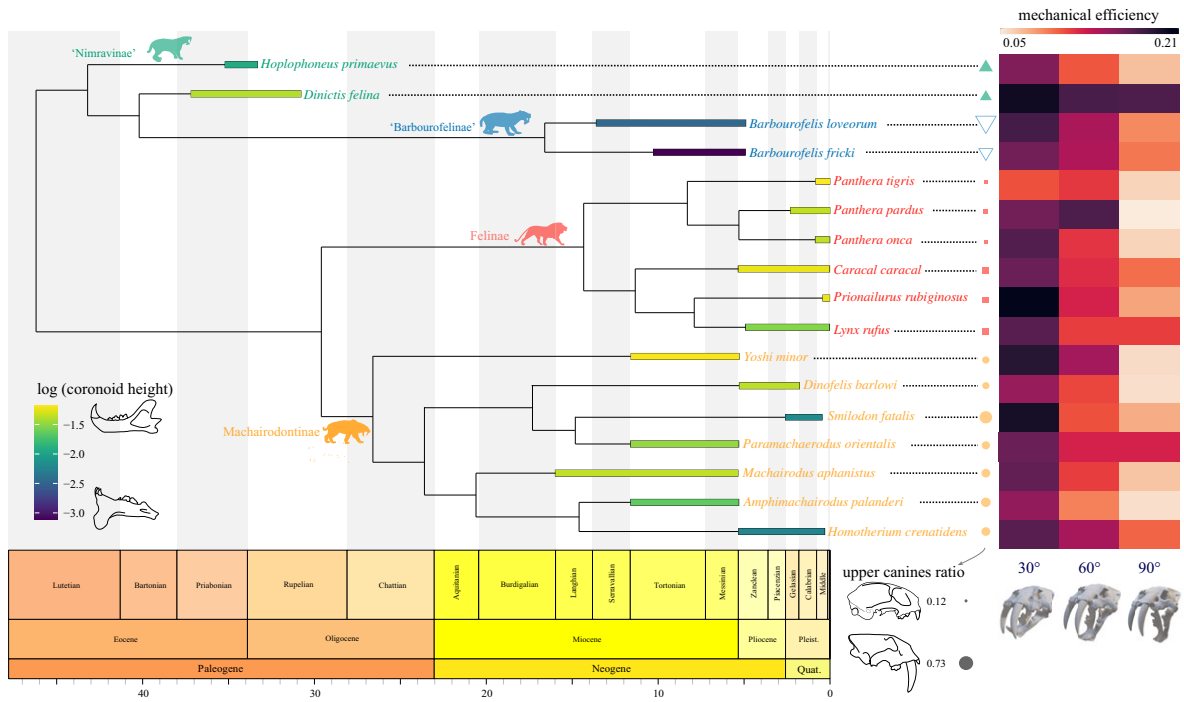


Figure 3. Phylogenetic relationships between the taxa studied with a continuous colour scale on the branches indicating the relative coronoid process height on a logarithmic scale, point size indicating the relative upper canine size and a heatmap showing the evolution of the mechanical efficiency at the three different angles. Abbreviations: Quat., Quaternary; Pleist., Pleistocene. (Online version in colour.)

Table 2. Results obtained with the phylsig function for the mechanical efficiency and adjusted strain energy. Phylogenetic signal: none, low Pagel's lambda and non-significant p -value; weak, high Pagel's lambda or significant p -value; strong, high Pagel's lambda and significant p -value.

		Pagel's lambda	logL lambda	p -value	phylogenetic signal
mechanical efficiency	30°	6.6107×10^{-05}	38.6404	1	none
	60°	0.102307	35.4671	0.857013	none
	90°	6.6107×10^{-05}	26.3708	0.046496	weak
adj. strain energy	30°	6.6107×10^{-05}	36.1021	1	none
	60°	6.6107×10^{-05}	31.6723	1	none
	90°	0.661484	41.0728	0.385862	weak

analyses suggested the existence of an additional, somewhat transitional, and pantherine-like killing method for homotherines and metailurines [16], as well as for the early machairodontines *Machairodus* and *Promegantereon* [17]. Our results demonstrate that some taxa belonging to typical sabre-tooth clades clearly differ from one another in terms of mandibular von Mises stress, suggesting that some taxa deviated from the canine shear bite and from the feline bite. Distinct mechanical responses are seen in sympatric taxa [53], such as *Hoplophoneus primaevus* + *Dinictis felina*; *Yoshi minor* + *Amphimachairodus palanderi*, possibly suggesting niche partitioning in feeding mechanics. Also, while the larger gape of sabre-tooths is usually interpreted as a hunting adaptation to use the elongated upper canines stabilizing the prey with the lower canines and incisors [3,6], a consistent drop in stress for lower carnassial bites could suggest that feeding mechanics in sabre-tooths is also more favourable at higher gapes. In other words, mandibular modifications of sabre-tooths may also have passively favoured carnassial food processing at larger gapes as well, not solely canine killing bites.

(b) Shorter coronoid process means larger gape and less stress

Within felines, the von Mises stress measured in the mandible was higher in smaller taxa within the same clade, which is not especially the case in other previous FEA studies, e.g. in otters [25], ungulates [54] or lizards [55]. It was already noted [11] that the largest amount of skull shape variation in felines is driven by allometry over functional or phylogenetic factors while in sabre-tooths the best predictor was canine length over body size [11]. Extant felids are mostly solitary ambush predators (except for the lion, *Panthera leo*) that bite their prey either in the throat, neck or sometimes the skull [56,57]. In this context, larger gapes expand the range of possible prey size, although field studies show that large species do not focus exclusively on large prey [58]. In extant taxa, gape angle tends to increase non-linearly with body size; the largest species appearing 'overbuilt' [59], in order to allow submission of large, energetic prey. Our results followed the same allometric relationship, as the crania of large feline taxa handle stress better than the

smaller ones. Indeed, in our dataset smaller felines (e.g. *Prionailurus rubiginosus*, *Caracal caracal*) have more gracile mandibles than the largest ones (e.g. *Panthera tigris*, *Panthera onca*) which clearly have an impact on the biomechanical behaviour of the mandible as seen in our von Mises stress contour plots (figure 1). There is a visible relationship between von Mises stress and upper canine height or coronoid process height (figure 2; electronic supplementary material, figure S19–S21), whose *R* squared values are affected by a couple of unusual taxa [11]. This actually contradicts a previous study using two-dimensional biomechanical simulations on cat-like mandibles that showed that stress is higher in sabre-toothed in the coronoid process but this could be explained by the different models used (two-dimensional data extracted from pictures or three-dimensional models) [19]. Also, sabre-toothed taxa better handle the torsion induced when biting at large gape with low values of stress on the balancing side which may be explained by the reduction of the size of the coronoid processes and general mandibular shape (figure 1). However, our dataset is not suited to fully test this assumption and specific tests would have to be done by including the modelling of mandibular symphysis materials, which are key to understand how torsional forces are transferred between hemimandibles [50]. Interestingly, the presence and development of the mandibular flange do not seem to affect any of the performance variables measured in our analyses, thereby questioning its functional importance in biting. It was suggested quite early [60] that those flanges protected the upper canines from lateral pression when the jaw was closed. Our analyses showing that it has no implication during biting and thus could support this assumption although this still does not explain why taxa with extremely elongated upper canines like *Smilodon* do not exhibit such flanges. Surprisingly, the von Mises stress values of felines strongly decreases at a 90° angle while this gape is mechanically impossible in this clade due to the size of the coronoid process and the curvature of post glenoid processes. The decline in stress values in all taxa at a 90° can be perhaps simply explained by the position of the biting points and the orientation of the muscle pulling the mandible resulting in a moderate stress in the mandibular corpus due to the poor lever arm. At 90°, the muscle vectors have a better alignment with the long axis of the mandible. Thus, sabre-tooths did not necessarily need specialized morphology to make the mandible any stronger at high gape; the main morphological change was instead to reduce the coronoid process to allow such jaw opening.

(c) Efficiency and strain energy are insensitive to sabre-tooth morphology

It is almost impossible to differentiate clades (Felines, machairodontines, nimravines or barbourufelines), families (Felids or nimravids), and morphotypes (sabre-tooth versus non-sabre-tooth) based on their adjusted strain energy (adj SE), their mechanical efficiency (ME), at the different angles or in the pattern of evolution of ME and adj SE from 30° to 90° (figure 3; electronic supplementary material, figures S21–S26; see MANOVA results above). A weak phylogenetic signal is present in our mechanical efficiency and adjusted strain at a 90° bite (table 2) possibly due to the particularly high ME in barbourufelines at this gape. This means

in effect that mandibular performance is insensitive to sabre-tooth morphology or phylogenetic relationships.

This unexpected result is particularly important because a wide series of unrelated clades have evolved elongated upper canines, ever since the Permian. When carnivorous, these taxa are often called sabre-tooth (e.g. thylacosmilids, gorgonopsians, biarmosuchians, anteosaurid dinocephalians) but many other clades have evolved comparable dental morphologies, such as the extant musk deer, chevrotains, the walrus, the Eocene, rhino-like Uintatheriidae [2,4,16,61–65], even bony fish [66]. The potential functions of elongated canines or caniniform teeth range from display, defence, intraspecific aggression, sexual selection, manipulation of food and the hunting of large prey items [2]. While the exact function remains obscure for some clades, especially in herbivorous extinct taxa [67], the presence of sabre teeth in carnivorous animals is often presented as an adaptation to kill large prey [2,3]. This wide array of possible functions indicates that multiple evolutionary drivers channelled the acquisition of elongated canines. Our results markedly add to this complexity by demonstrating a functional decoupling between canine elongation and mandible performance in the iconic sabre-toothed carnivoran mammals.

Finally, as predicted by Wainwright *et al.* [68] the ‘many-to-one mapping’ of form–function relationships can be applied to various complex biological systems; the cat-like mandible now appears as a striking example of such a phenomenon, displaying a high morphological disparity with little mechanical variation in terms of mechanical efficiency and adjusted strain energy. This was not expected after the results published by Lautenschlager *et al.* [16] wherein all the analysed functional parameters (actual and effective gape angle, bending strength, bite force) show a continuum distribution of results between the two morphotypes. The similarities in terms of mechanical efficiency and adjusted strain energy could be due to similar canine clearance during the bite. Indeed, forms with smaller upper canines biting at a 30° angle might have a similar canine clearance to extremely derived sabre-tooth like *Smilodon fatalis* or *Barbourufelis fricki* at a 90° gape angle. Still, our results highlighted a continuum in terms of stress distribution in the cat-like mandible possibly suggesting a wide range of hunting methods in those carnivorans.

5. Conclusion

We thoroughly analysed the biomechanical behaviour of mandibles of cat-like taxa, extant and extinct, under multiple biting scenarios. Our analyses show a better stress repartition in taxa with long upper canines with a global stress decreasing at larger gape angles which corroborate that those species are adapted to bite at larger angles. However, we show a continuous spectrum of mechanical responses in terms of mechanical efficiency and adjusted strain energy in the cat-like mandibles rather than a discrete difference between sabre-tooth and non-sabre-tooth forms. Despite striking morphological differences within felines, machairodontines, nimravines and barbourufelines, their mandibular architectures react similarly in a mechanical efficiency and strain energy framework. This indicates a spectrum of hunting methods in cat-like carnivorans rather than a two-peaked adaptive landscape, as forces involved in those different hunting scenarios were not drastically variable. Also, this points out that the cat-like mandible

in its non-sabre-tooth forms was already mechanically strong and able to endure a bite at an extremely large angle (90°) meaning that all the morphological variations associated with the sabre-tooth ecomorphs are only meant to make that bite possible and not to build a stronger mandible to support that bite.

Data accessibility. All three-dimensional models used to perform the FEA are available on MorphoSource (Project ID: 000473875, <https://www.morphosource.org/projects/000473875/>). Excel files containing the model properties, raw results, calculation of the adjusted strain energy and mechanical efficiency, final Strand7 loaded files, the modified MATLAB code as well as the R script used to create the plots and perform the statistical tests are provided as supplementary files and are available on Orbi, the ULiège Open Repository (<https://hdl.handle.net/2268/296076>).

The data are provided in electronic supplementary material [69].

Authors' contributions. N.C.: conceptualization, data curation, formal analysis, funding acquisition, investigation, methodology, project administration, visualization, writing—original draft, writing—review and editing; V.F.: conceptualization, funding acquisition, supervision, writing—review and editing; Z.J.T.: conceptualization, funding acquisition, methodology, resources, software, supervision, writing—original draft, writing—review and editing.

All authors gave final approval for publication and agreed to be held accountable for the work performed therein.

Conflict of interest declaration. We declare we have no competing interests.

Funding. N.C. is supported by a grant of Fonds de la Recherche Scientifique FRS–FNRS (FRIA grant no. FRIA FC 36251). V.F. is supported by a grant of Fonds de la Recherche Scientifique FRS–FNRS (grant no. MIS F.4511.19). Z.J.T. is supported by NSF (grant no. DBI 2128146).

Acknowledgments. We are extremely thankful to all curators, collection managers and staff, whose help and support was fundamental to collect all the scans we needed to perform this study. Especially, we would like to thank: Geraldine Véron (MNHN, Paris, France), Daniela Kalthoff and Thomas Mörs (NRM, Stockholm, Sweden), Benjamin Kear (PMU, Uppsala, Sweden), Roula Pappa and Pip Brewer (NHMUK, London, United Kingdom), Patricia Holroyd (UCMP, Berkeley, USA), Samuel A. McLeod and Xiaoming Wang (NHMLA, Los Angeles). We would also like to show our gratitude to Florent Gousard and Christine Argot (MNHN, Paris, France) for providing us structured light scan and CT scans of *Homotherium crenatidens*. For access to the surface scan data of *Dinofelis barlowi*, we thank the Ditsong National Museum of Natural History, South Africa, and Justin Adams of the Department of Anatomy and Developmental Biology, Monash University, Australia. We are also extremely thankful to Jeanette Pirlo and Sierra Steely for the surface scans of the holotype of *Barbourofelis loveorum* from the University of Florida. We are immensely grateful to Romain Boman from the Aerospace & Mechanical Engineering department in the University of Liège for his help to improve the forces distribution in the 'Boneload' MATLAB routine. Finally, we would like to thank John Hutchinson as well as three anonymous reviewers for their constructive comments on a previous version of the manuscript.

References

- Turner A, Antón M, Salesa MJ, Morales J. 2011 Changing ideas about the evolution and functional morphology of machairodontine felids. *Estudios Geológicos* **67**, 255–276. (doi:10.3989/egol.40590.188)
- Anton M. 2013 *Sabertooth*. Bloomington, IL: Indiana University Press.
- Emerson SB, Radinsky L. 1980 Functional analysis of sabertooth cranial morphology. *Paleobiology* **6**, 295–312. (doi:10.1017/S0094837300006813)
- van Valkenburgh B, Jenkins I. 2002 Evolutionary patterns in the history of Permo-Triassic and Cenozoic synapsid predators. *Paleontol. Soc. Pap.* **8**, 267–288. (doi:10.1017/s108933260001121)
- Gonyea WJ. 1976 Adaptive differences in the body proportions of large felids. *Acta Anat (Basel)* **96**, 81–96. (doi:10.1159/000144663)
- Akersten WA. 1985 Canine function in Smilodon (Mammalia, Felidae, Machairodontinae). *Contrib. Sci.* **356**, 1–22. (doi:10.5962/p.226830)
- Turner A, Antón M. 1997 *The big cats and their fossil relatives: an illustrated guide to their evolution and natural history*. New York, NY: Columbia University Press.
- Antón M, Galobart À. 1999 Neck function and predatory behavior in the scimitar toothed cat *Homotherium latidens* (Owen). *J. Vertebr. Paleontol.* **19**, 771–784. (doi:10.1080/02724634.1999.10011190)
- Argot C. 2004 Functional-adaptive features and palaeobiologic implications of the postcranial skeleton of the late Miocene sabertooth borhyaenoid thylacosmilus atrox (Metatheria). *Alcheringa* **28**, 229–266. (doi:10.1080/03115510408619283)
- Andersson K, Norman D, Werdelin L. 2011 Sabretoothed carnivores and the killing of large prey. *PLoS ONE* **6**, e24971. (doi:10.1371/journal.pone.0024971)
- Slater GJ, van Valkenburgh B. 2008 Long in the tooth: evolution of sabertooth cat cranial shape. *Paleobiology* **34**, 403–419. (doi:10.1666/07061.1)
- Martin LD, Babiarczyk JP, Naples VL, Hearst J. 2000 Three ways to be a saber-toothed cat. *Naturwissenschaften* **87**, 41–44. (doi:10.1007/s001140050007)
- Matthew WD. 1910 The phylogeny of the felidae. *Bull. Am. Mus. Nat. Hist.* **28**, 289–318. (doi:10.1007/bf01798035)
- Figueirido B, MacLeod N, Krieger J, de Renzi M, Pérez-Claros JA, Palmqvist P. 2011 Constraint and adaptation in the evolution of carnivoran skull shape. *Paleobiology* **37**, 490–518. (doi:10.1666/09062.1)
- Figueirido B, Lautenschlager S, Pérez-Ramos A, van Valkenburgh B. 2018 Distinct predatory behaviors in scimitar- and dirk-toothed sabertooth cats. *Curr. Biol.* **28**, 3260–3266.e3. (doi:10.1016/j.cub.2018.08.012)
- Lautenschlager S, Figueirido B, Cashmore DD, Bendel EM, Stubbs TL. 2020 Morphological convergence obscures functional diversity in sabretoothed carnivores: sabre-tooth functional morphology. *Proc. R. Soc. B* **287**, 20201818. (doi:10.1098/rspb.2020.1818)
- Chatar N, Fischer V, Siliceo G, Antón M, Morales J, Salesa MJ. 2021 Morphometric analysis of the mandible of primitive sabretoothed felids from the late Miocene of Spain Madrid. *J. Mamm. Evol.* **28**, 753–771. (doi:10.1007/s10914-021-09541-0)
- McHenry CR, Wroe S, Clausen PD, Moreno K, Cunningham E. 2007 Supermodeled sabercat, predatory behavior in Smilodon fatalis revealed by high-resolution 3D computer simulation. *Proc. Natl Acad. Sci. USA* **104**, 16 010–16 015. (doi:10.1073/pnas.0706086104)
- Piras P, Maiorino L, Teresi L, Meloro C, Lucci F, Kotsakis T, Raia P. 2013 Bite of the cats: Relationships between functional integration and mechanical performance as revealed by mandible geometry. *Syst. Biol.* **62**, 878–900. (doi:10.1093/sysbio/syt053)
- Janis CM, Figueirido B, DeSantis L, Lautenschlager S. 2020 An eye for a tooth: Thylacosmilus was not a marsupial 'saber-tooth predator'. *PeerJ* **2020**, 1–36. (doi:10.7717/peerj.9346)
- Bourke J, Wroe S, Moreno K, McHenry C, Clausen P. 2008 Effects of gape and tooth position on bite force and skull stress in the dingo (*Canis lupus dingo*) using a 3-dimensional finite element approach. *PLoS ONE* **3**, e2200. (doi:10.1371/journal.pone.0002200)
- Oldfield CC, McHenry CR, Clausen PD, Chamoli U, Parr WCH, Stynder DD, Wroe S. 2012 Finite element analysis of ursid cranial mechanics and the prediction of feeding behaviour in the extinct giant *Agriotherium africanum*. *J. Zool.* **286**, 171. (doi:10.1111/j.1469-7998.2011.00862.x)
- Cox PG, Rinderknecht A, Blanco RE. 2015 Predicting bite force and cranial biomechanics in the largest fossil rodent using finite element analysis. *J. Anat.* **226**, 215–223. (doi:10.1111/joa.12282)
- Tsong ZJ, Grohé C, Flynn JJ. 2016 A unique feeding strategy of the extinct marine mammal

- kolonomos: convergence on sabretooths and sea otters. *Proc. R. Soc. B* **283**, 20160044. (doi:10.1098/rspb.2016.0044)
25. Tseng ZJ, Su DF, Wang X, White SC, Ji X. 2017 Feeding capability in the extinct giant *Siamogale melilutra* and comparative mandibular biomechanics of living Lutrinae. *Sci. Rep.* **7**, 1–10. (doi:10.1038/s41598-017-15391-9)
26. Lautenschlager S, Gill P, Luo ZX, Fagan MJ, Rayfield EJ. 2017 Morphological evolution of the mammalian jaw adductor complex. *Biol. Rev.* **92**, 1910–1940. (doi:10.1111/brv.12314)
27. Püschel TA, Marcé-Nogué J, Gladman JT, Bobe RR, Sellers WI. 2018 Inferring locomotor behaviours in Miocene New World monkeys using finite element analysis, geometric morphometrics and machine-learning classification techniques applied to talar morphology. *J. R. Soc. Interface* **15**, 20180520. (doi:10.1098/rsif.2018.0520)
28. Rowe AJ, Rayfield EJ. 2022 The efficacy of computed tomography scanning versus surface scanning in 3D finite element analysis. *PeerJ* **10**, e13760. (doi:10.7717/PEERJ.13760/SUPP-1)
29. Wroe S, McHenry C, Thomason J. 2005 Bite club: comparative bite force in big biting mammals and the prediction of predatory behaviour in fossil taxa. *Proc. R. Soc. B* **272**, 619–625. (doi:10.1098/RSPB.2004.2986)
30. Dessem D, Druzinsky RE. 1992 Jaw-muscle activity in ferrets, *Mustela putorius furo*. *J. Morphol.* **213**, 275–286. (doi:10.1002/jmor.1052130211)
31. Currey JD. 1987 The evolution of the mechanical properties of amniote bone. *J. Biomech.* **20**, 1035–1044. (doi:10.1016/0021-9290(87)90021-2)
32. Currey JD, Brear K. 1990 Hardness, Young's modulus and yield stress in mammalian mineralized tissues. *J. Mater. Sci. Mater. Med.* **1**, 14–20. (doi:10.1007/BF00705348)
33. Gill PG, Purnell MA, Crumpton N, Brown KR, Gostling NJ, Stampanoni M, Rayfield EJ. 2014 Dietary specializations and diversity in feeding ecology of the earliest stem mammals. *Nature* **512**, 303–305. (doi:10.1038/nature13622)
34. Erickson GM, Catanese J, Keaveny TM. 2002 Evolution of the biomechanical material properties of the femur. *Anatomic. Rec.* **268**, 115–124. (doi:10.1002/ar.10145)
35. Grosse IR, Dumont ER, Coletta C, Tolleson A. 2007 Techniques for modeling muscle-induced forces in finite element models of skeletal structures. *Anatomic. Rec.* **290**, 1069–1088. (doi:10.1002/ar.20568)
36. Dumont ER, Davis JL, Grosse IR, Burrows AM. 2011 Finite element analysis of performance in the skulls of marmosets and tamarins. *J. Anat.* **218**, 151–162. (doi:10.1111/j.1469-7580.2010.01247.x)
37. R Core Team. 2021 *R: a language and environment for statistical computing*. Vienna, Austria: R Foundation for Statistical Computing.
38. Wickham H. 2007 Reshaping Data with the reshape Package. *J. Stat. Softw.* **21**, 1–20. (doi:10.18637/jss.v021.i12)
39. Zeileis A, Grothendieck G, Ryan JA, Ulrich JM, Andrews F. 2022 Package 'zoo'. See <https://cran.r-project.org/web/packages/zoo/index.html>.
40. Revell LJ. 2012 phytools: An R package for phylogenetic comparative biology (and other things). *Methods Ecol. Evol.* **3**, 217–223. (doi:10.1111/j.2041-210X.2011.00169.x)
41. Bapst DW. 2012 paleotree: an R package for paleontological and phylogenetic analyses of evolution. *Methods Ecol. Evol.* **3**, 803–807. (doi:10.1111/j.2041-210X.2012.00223.x)
42. Bell MA, Lloyd GT. 2015 strap: an R package for plotting phylogenies against stratigraphy and assessing their stratigraphic congruence. *Palaeontology* **58**, 379–389. (doi:10.1111/PALA.12142)
43. Yu G, Smith DK, Zhu H, Guan Y, Lam TTY. 2017 ggtree: an r package for visualization and annotation of phylogenetic trees with their covariates and other associated data. *Methods Ecol. Evol.* **8**, 28–36. (doi:10.1111/2041-210X.12628)
44. Wickham H. *et al.* 2016 Package ggplot2: create elegant data visualisations using the grammar of graphics. See <https://ggplot2.tidyverse.org/>.
45. Kassambara A. 2020 ggpubr. See <https://github.com/kassambara/ggpubr>.
46. Paradis E, Schliep K. 2019 Ape 5.0: An environment for modern phylogenetics and evolutionary analyses in R. *Bioinformatics* **35**, 526–528. (doi:10.1093/bioinformatics/bty633)
47. Barrett PZ. 2021 The largest hoplophorine and a complex new hypothesis of nimravid evolution. *Sci. Rep.* **11**, 1–9. (doi:10.1038/s41598-021-00521-1)
48. Jiangzuo Q, Werdelin L, Sun Y. 2022 A dwarf sabretooth cat (Felidae: Machairodontinae) from Shanxi, China, and the phylogeny of the sabretooth tribe Machairodontini. *Quat. Sci. Rev.* **284**, 107517. (doi:10.1016/j.quascirev.2022.107517)
49. Slater GJ, Friscia AR. 2019 Hierarchy in adaptive radiation: a case study using the Carnivora (Mammalia). *Evolution (N Y)* **73**, 524–539. (doi:10.1111/evo.13689)
50. Tseng ZJ, Stynder D. 2011 Mosaic functionality in a transitional ecomorphology: skull biomechanics in stem Hyaininae compared to modern South African carnivorans. *Biol. J. Linnean Soc.* **102**, 540–559. (doi:10.1111/j.1095-8312.2010.01602.x)
51. Greaves WS. 1982 A mechanical limitation on the position of the jaw muscles of mammals: the one-third rule. *J. Mammal.* **63**, 261–266. (doi:10.2307/1380635)
52. Anyonge W. 1996 Locomotor behaviour in Plio-Pleistocene sabre-tooth cats: a biomechanical analysis. *J. Zool* **238**, 395–413. (doi:10.1111/J.1469-7998.1996.TB05402.X)
53. Van Valkenburgh B. 1999 Major patterns in the history of carnivorous mammals. *Annu. Rev. Earth Planet Sci.* **27**, 463–493. (doi:10.1146/annurev.earth.27.1.463)
54. Zhou Z, Winkler DE, Fortuny J, Kaiser TM, Marcé-Nogué J. 2019 Why ruminating ungulates chew sloppily: biomechanics discern a phylogenetic pattern. *PLoS ONE* **14**, e0214510. (doi:10.1371/JOURNAL.PONE.0214510)
55. McCurry MR, Mahony M, Clausen PD, Quayle MR, Walmsley CW, Jessop TS, Wroe S, Richards H, McHenry CR. 2015 The relationship between cranial structure, biomechanical performance and ecological diversity in varanoid lizards. *PLoS ONE* **10**, e0130625. (doi:10.1371/JOURNAL.PONE.0130625)
56. Ewer RF. 1998 *The carnivores*. Ithaca, NY: Cornell University Press.
57. Leyhausen P. 1979 *Cat behaviour: the predatory and social behaviour of domestic and wild cats*, 1st edn. New York, NY: Garland STPM Press.
58. Radloff FGT, Du Toit JT. 2004 Large predators and their prey in a southern African savanna: a predator's size determines its prey size range. *J. Anim. Ecol.* **73**, 410–423. (doi:10.1111/j.0021-8790.2004.00817.x)
59. Slater GJ, Van Valkenburgh B. 2009 Allometry and performance: the evolution of skull form and function in felids. *J. Evol. Biol.* **22**, 2278–2287. (doi:10.1111/j.1420-9101.2009.01845.x)
60. Berryman Scott W, Lowell Jepsen G. 1936 The mammalian fauna of the white river oligocene: part I. Insectivora and Carnivora. *Trans. Amer. Phil. Soc.* **28**, 1–153. (doi:10.2307/1005507)
61. Bubenik GA, Bubenik AB. 1990 *Horns, pronghorns, and antlers*. New York, NY: Springer.
62. Ivakhnenko MF. 2008 Cranial morphology and evolution of Permian Dinomorpha (Eotherapsida) of eastern Europe. *Paleontol. J.* **42**, 859–995. (doi:10.1134/S0031030108090013)
63. Ivakhnenko MF. 2005 Morphology of the Gorgonopidae (Eotherapsida) and Tetrapod communities in the Late Paleozoic. *Paleontol. J.* **39**, S393–S511.
64. Rubidge BS, Sidor CA. 2001 Evolutionary patterns among permo-triassic therapsids. *Annu. Rev. Ecol. Syst.* **32**, 449–480. (doi:10.1146/annurev.ecolsys.32.081501.114113)
65. Leinders JMM, Heintz E. 1980 Historical notes on the taxonomy and nomenclature of the recent Rhinocerotidae (Mammalia. Perissodactyla). *Beaufortia* **30**, 155–160.
66. Capobianco A, Beckett HT, Steurbaut E, Gingerich PD, Carnevale G, Friedman M. 2020 Large-bodied sabretoothed anchovies reveal unanticipated ecological diversity in early Palaeogene teleosts. *R. Soc. Open Sci.* **7**, 192260. (doi:10.1098/rsos.192260)
67. Cisneros JC, Abdala F, Rubidge BS, Dentzien-Dias PC, de Oliveira Bueno A. 2011 Dental occlusion in a 260-million-year-old therapsid with saber canines from the permian of Brazil. *Science (1979)* **331**, 1603–1605. (doi:10.1126/science.1200305)
68. Wainwright PC, Alfaro ME, Bolnick DI, Husley CD. 2005 Many-to-one mapping of form to function: a general principle in organismal design? *Integr. Comp. Biol.* **45**, 256–262. (doi:10.1093/icb/45.2.256)
69. Chatar N, Fischer V, Tseng ZJ. 2022 Data from: Many-to-one function of cat-like mandibles highlights a continuum of sabre-tooth adaptations. Figshare. (doi:10.6084/m9.figshare.c.6308901)